Atomistic resolution structure and dynamics of lipid bilayers in simulations and experiments

O. H. Samuli Ollila[1,*]
[1]Aalto University
(Dated: November 10, 2015)

Recent progress in the analysis of lipid bilayer atomistic resolution structure and dynamics using combination of robust experimental data and molecular dynamics simulations is reviewed. The focus is on order parameters and spin relaxation times measured with NMR and on form factors measured with SAXS and SANS for phosphatidylcholine lipid bilayers. The experimental observables are chosen since these experiments are robust, well understood, highly reproducible and the connection between raw data and simulations is straightforward. Also the comparison between simulations and these observables is bidirectionally useful; it will quantitatively measure the quality of the simulation model respect to the reality, and if the quality is sufficient, the simulations give structural interpretation for the experimental data. Significant advance of molecular dynamics simulation models is that the same simulation model can be simultaneously compared to all of this parameters. If satisfactory agreement is found, it is highly likely that the model represents the reality due to the large amount of reproduced independent experimental parameters. In this case all the mentioned experiments would be simultaneously interpreted with the same model. Phosphatidylcholine lipids are chosen since large portion of model membrane studies have been focused on this lipid, producing enough experimental and simulation data to draw comprehensive picture on the level of understanding atomistic resolution structure and dynamics. We conclude that the acyl chain region structure and its changes are generally well described in simulations, in contrast to the glycerol backbone and choline. Also cation binding is significantly overestimated by several models.

INTRODUCTION

1.Citations missing Atomistic resolution structure and dynamics of lipid bilayers has been studied with wide range of techniques for many decades motivated mainly by their presence and important role in biological systems [1**?** –5]. Lipid bilayers play direct or indirect role in several physiological and pathological molecular scale processes [6**?** , 7]. To fully understand these processes the atomistic and molecular level understanding of lipids is required. Since atomistic resolution studies are extremely difficult from biological samples, purified lipid systems are often used [**?**]. The biological relevance of these model systems is supported, e.g. by similar NMR order parameters mesured from living cells, lipid extracts and model systems [**?**].

The most detailed information about lipid bilayer atomistic resolution structure and dynamics has been achieved with various Nuclear Magnetic Resonance (NMR) and scattering techiques [2**?** –5]. The first one giving direct information on structures sampled by individual lipid molecules [2**?** –4] and the latter one giving complementary information on average bilayer properties, like density and thickness [5**?**]. Both techniques give robust, accurate and reproducible quantities related to the strucuture and dynamics. However, for structural and dynamical interpretation both techniques needs a model which reproduces the measured quantities [2**?** –5].

On the other hand, remarkable progress in hardware and software has made possible to routinely perform classical atomistic resolution molecular dynamics (MD) simulations of lipid bilayer with duration of tens or hundreds nanoseconds. Ideally the molecules are sampling realistic conformations with realistic speed in these simulations. This can be verified by calculating directly measurable quantities from simulations and comparing these to experimental values. Here we review such comparisons for different experimental observables: C–H bond order parameters, spin relaxation times and form factor. The first and second are measured with NMR thus they represent to structure and dynamics sampled by individual lipid molecules, respectively. The last is measured with scattering techniques and represents the bilayer average properties.

The order parameters and spin lattice relaxation times have been compared between simulations and experiments for validation and interpretation since the early days of lipid MD simulations [8, 9]. On the other hand, scattering form factors for lipid bilayers have been replacing the comparisons of simulations to the experimental area per molecule during the last decade since form factor is directly measurable quantity while area per molecule value depends on model used to analyze the scattering data [5].

If an atomistic resolution model reproduces all the above mentioned experimental parameters, i.e. order parameters, spin relaxation rates and form factor, the simulation can be considered as an ultimate model giving interpretation for all these experiments simulatenously. In addition, it would be the correct atomistic resolution representation of the system with high probability since it reproduces large amount of indepedetly measured experimental parameters simultaneously. Thus, the model usage of the for further applications would be well justified.

Here we review recent studies comparing the order parameters, spin relaxation rates and scattering form factors between experiments and simulations in order to quantify the quality of simulation models and interpret the experiments. Also relevat techical details on experimental data and simulation analysis is reviewed. We focus on phosphatidylcholine lipid bilayers due to most comprehensive available datasets for both, simulations and experiments. However, the basic ideas of the approach is valid also for other lipids and surfactants and there

is also data and literature available [**?**]. We also discuss the observed structural changes of lipids induced by external conditions and their relation, e.g. to ion partition. We pay special attention on the accuracy and usability of the NMR order parameter data which is often underestimated in the literature, especially for the glycerol backbone and choline regions.

The general conclusion from the review is that the hydrophopic acyl chain region is well described in simulation models and the atomistic resolution interpretation of experiments has been successfull for this region. However, the glycerol backbone and choline regions are less well described in simulation models which may question their usability in studies where this region is important.

The structural details of the these segments are potentially relevant in several biochemical applications of atomistic resolution lipid bilayer simulations. For example, interactions between lipid bilayer with ions, drug molecules or proteins may be dependent on the detailed headgroup structure. Due to the large variation of lipid headgroups present in biological systems, its chemical details are most likely important at least for some physiological processes. One goal of this review is to demonstrate how model quality can be estimated to minimize possibility of artificial conclusions made from simulation studies.

C-H BOND ORDER PARAMETERS AS ATOMISTIC RESOLUTION STRUCTURAL MEASURE

2.The text should be close to final. Figures should be improved.

Definition and properties of C-H bond order parameter

In lipid bilayer systems the order parameter of a hydrocarbon C–H vector is typically defined as

$$S_{\mathrm{CH}} = \frac{1}{2}\langle 3\cos^2\theta - 1\rangle, \qquad (1)$$

where the angle brackets denote an ensemble average over the sampled conformations, and θ is the angle between the C–H bond and the membrane normal. The numerical values of order parameters vary between $-\frac{1}{2} < S_{\mathrm{CH}} < +1$ depending on the sampled θ distribution. The definition is motivated by its connection to the dipolar and quadrupolar splitting measured with ^{1}H-^{13}C and ^{2}H NMR techniques, respectively. The functional form comes from the fundamental theory of interactions between spin systems which gives a connection between average molecules orientations and NMR measurables [10].

If the sampled distribution of θ for a C–H bond are known, the order parameter can be straighfowardly calculated from Eq. 1. However, the sampled θ distribtions cannot be uniquely determined from the known order parameter. Thus the experimental order parameter values gives a set of conditions which structural molecular model (more specifically the C–H bond vectors of the model) has to fulfill but the experimental order parameters alone cannot be used to uniquely resolve the structure. The same applies practically to all experimental parameters used in biomolecular structure determination.

Atomistic resolution molecular dynamic simulations naturally produces the sampled structures and the calculated θ distributions can be substituted into Eq. 1 to calculate the order parameters. If and only if the experimental order parameters are reproduced, the sampled structures can be considered as a realistic atomistic resolution representation and used to interpretate experimental order parameters. Before MD simulations were feasible for such usage, other models have been used for this interpretation [11–18]. It is important to note, however, that reproduction of the order parameters does not absolutely guarantee that the sampled structures are correct since several structural models can produce the same order parameters, in principle. Significant advance of the MD models compared to the traditional models is that the same MD structures can be straightforwardly compared to other experimental observables in addition to order parameters, like ^{31}P chemical shift anisotropy [19], ^{31}P-^{13}C dipolar couplings [20], spin relaxation data [21] and scattering data [22]. The comparisons of the same model to the various independently measured experimental observables significantly reduces the possibility of getting unrealistic structures reproducing correct order parameters.

The probability for unrealistic structures is further reduced by the large amount of experimentally available order parameter values. As discussed in this review, the order parameters can be measured with high accuracy for each C–H pair of a lipid molecule in a liquid crystalline bilayer [2, 3, 23–27]. Also the signs [17, 24, 28] and stereospecifity of C–H segments in the same carbon (*forking*) [24–26, 29–31] are experimentally available. Consequently, a realistic atomistic resolution model, for example, for POPC molecule (see Fig. 1 B)) in liquid crystalline bilayer has to reproduce 82 experimental order parameter values. If these parameters are not reproduced for certain segments, the model deficiencies are easy to localize since order parameter is very local quantity depending only on the position of two atoms (C-H pair). This is an advance over several other accurately measured NMR quantities depending on the position of several atoms [19, 20], thus complicating the localization of strucutral differences in the case of disagreement between model and experiments.

Experimental order parameter data for single component lipid bilayers is very well available in the literature [26, 27, 48–53]. The amount of data, especially from ^{13}C NMR, has been also increasing lately [26, 48, 49, 52, 53]. Also changes of order parameters for all lipid segments has been measured respect to several different conditions, like temperature [**?**], hydration level [25, 34, 54, 55] and due to the presense of ions and charged objects [33, 56–58], cholesterol [26, 53, 59, 60] and proteins [52, 61, 62]. The comparison of order parameter responses between experiments and simulations has not been much utilized in the literature, thus we will exemplify its potential by showing the Na+ ion effect on choline order pa-

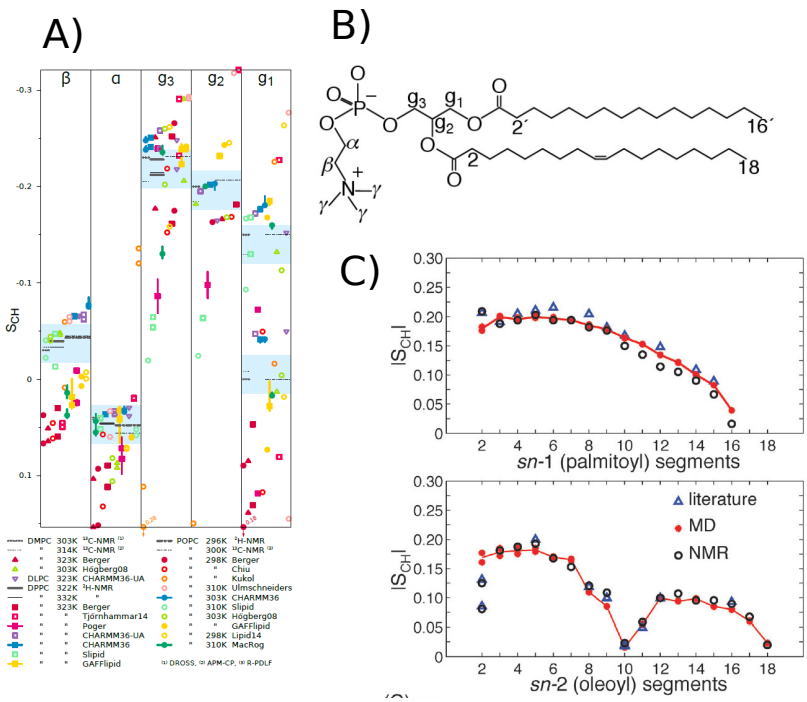

FIG. 1: A) Order parameters from simulations and experimens for phosphatidylcholine headgroup and glycerol backbone segments adapted from Botan et al. [27]. The blue shaded regions show the subjective sweetspots where the simulation data should fall to agree with experiments, based on estimated quantitative accuracy of order parameter measurements by Botan et al. B) Chemical structure of 1-palmitoyl-2-oleoylphosphatidylcholine (POPC). C) Order parameters $|S_{\mathrm{CH}}|$ for POPC acyl chains from ^{1}H-^{13}C NMR at 300K (black dots) [26], from ^{2}H NMR at 300K (blue triangles, literature) [14, 32] and from MD simulations at 298K (red dots) [26]. The experimental values shown in A): DMPC 303 K [24], DMPC 314 K [25], DPPC 322 K [12], DPPC 323 K [33], POPC 296 K [34], and POPC 300 K [26]. The force fields in A): Berger [35], Hogberg08 [36], Poger [37], Ulmschneiders [38], Kukol [39], Chiu [40], CHARMM36 [41], GAFFlipid [42], Slipid [43], MacRog [44], Tjörnhammar14 [45], Lipid14 [46], CHARMM36-UA [47]. The interactive version of this figure is available at https://plot.ly/∼HubertSantuz/72/lipid-force-field-comparison/.

rameters and its relation to ion partition in both, simulations [63] and experiments [33, 56–58].

In this work we discuss only order parameters directly measured from multilamellar samples which are closest experimental analogue to MD simulations with periodic boundary conditions. We do not discuss order parameters measured for other type of samples, e.g. bicelles [64–66], or indirect measurements by using, e.g. relaxation data [67] since the comparison to the standard simulation setup is less straightforward.

Order parameters from ^{2}H NMR experiments

The absolute values of order parameters are connected to the quadrupolar splitting $\Delta\nu_Q$ in ^{2}H NMR experiments through the equation

$$|S_{\mathrm{CD}}| = \frac{4}{3}\frac{h}{e^2 qQ}\Delta\nu_{\mathrm{Q}}, \tag{2}$$

where e is the elementary charge, Q is the deuteron quadrupole moment and h is the Planck's constant. The parameter q is related to the largest electric field gradient and in practise its value is not known; therefore the static quadrupolar coupling constant $\frac{e^2qQ}{h}$ is defined, and its value measured

for different compounds in their solid state ($\Delta\nu_Q$ measurement from the system where order parameter is known to be 1). In C-D order parameter measurements for lipids, it is typical to use the value measured for different alkenes, $\frac{e^2qQ}{h}$=170 kHz. The relation between order parameters and quadrupolar splittings then becomes $S_{\mathrm{CD}} = 0.00784 \times \Delta\nu_{\mathrm{Q}}$. This relation is useful as many publications report only the quadrupolar splittings. For a review and more accurate description see the work of Seelig [23].

For ^2H NMR measurements the CH_2 segments has to be labeled with deuterium. This can be done specifically for a certain segment or for the several segments simultaneously [3, 4, 50]. In the first case, it is known that the measured order parameter (quadrupolar splitting) is related to the labeled segment. In the latter case several order parameters (quadrupolar splittings) are measured which arise from all the labeled segments, however, it is not known which order parameter belongs to which CH_2 segment. Majority of the ^2H NMR data in the literature is measured from samples with perdeuterated acyl chain [50, 51] while also order parameter data from specifically deuterated lipids are available for several lipid types in various conditions [11, 13, 14, 29, 30, 33, 54, 56, 58, 60–62].

Order parameters from ^{13}C NMR experiments

The order parameter can be related to the dipolar splitting $\Delta\nu_{\mathrm{CH}}$ from ^{13}C-^{1}H NMR experiment which is related to the effective dipolar coupling d_{CH} through a scaling factor depending on the used pulse sequence [24–26, 28]. The effective dipolar coupling d_{CH} is then connected to the absolute value of order parameter through equation

$$|S_{\mathrm{CH}}| = (\frac{D_{\mathrm{max}}}{2\pi})^{-1} d_{\mathrm{CH}}, \tag{3}$$

where $D_{\mathrm{max}} = \frac{\hbar\mu_0\gamma_h\gamma_c}{4\pi\langle r_{\mathrm{CH}}^3\rangle}$. r_{CH} is the C-H distance, μ_0 is the vacuum permittivity, and γ_h and γ_c are the gyromagnetic constants for ^{1}H and ^{13}C nuclei. In contrast to Eq. 2, all the parameters in Eq. 3 are in principle known. However, for the internuclear distance only the average $\langle r_{\mathrm{CH}}\rangle$ is known, not the third moment $\langle r_{\mathrm{CH}}^3\rangle$. For this reason values between 20.2-22.7 kHz are used for $\frac{D_{\mathrm{max}}}{2\pi}$ depending on the original authors [21, 24–26, 28, 68].

In contrast to ^{2}H NMR specific labeling is not needed for ^{13}C NMR experiments due the natural abundance of ^{13}C, however it could be used to enhance the signal for specific segment under interest [69]. Order parameter measurements with ^{13}C NMR are 2D experiments, the chemical shift being in the first dimension and dipolar coupling in the second [24–26, 28]. The chemical shift depends on the local chemical environment and is different for each carbon segment. In the second dimension the dipolar coupling (order parameter) corresponding each chemical shift value is measured, and its value can be connected, in principle, to each carbon segment by using the chemical shift value. This is straighforward for hydrocarbon segments in choline, glycerol backbone, close to the double bonds, and in the beginning and the end of acyl chains due to their distinct chemical shift values [24–26, 28, 53]. Challenges occur in the acyl chain region where chemical shift values of different segments are very close to each others [24–26, 28, 53]. This issue has been solved by filtering the spectra by using partially deuterated lipids [26] and using data from simulations and previous specifically deuterated experiments to help in the assigment [26, 53].

Quantitative accuracy of experimental order parameter values

It must be stressed that ^{2}H NMR and ^{13}C NMR are fully independent experiments since the deuterium quadrupolar splitting $\Delta\nu_Q$ and the dipolar splitting d_{CH} are different physical observables. In addition, the prefactors connecting the observables to the order parameter (Eqs. 2 and 3) are independently measured. Further independent experiments are performed by measuring the ^{1}H-^{13}C dipolar couplings using different pulse sequences [24–26, 28] when the connection between dipolar splitting $\Delta\nu_{\mathrm{CH}}$ and effective dipolar coupling d_{CH} is different.

The measurements of quadrupole $\Delta\nu_Q$ and dipolar d_{CH} splittings are relatively accurate, especially for quadrupolar splitting. **3.How accurate exactly?** Thus the quantitative accuracy of measured order parameters is mainly determined by the prefactors connecting the splittings and order parameters in Eqs. 2 and 3. Since the prefactors are independently determined for the ^{2}H and ^{13}C NMR measurements, the quantitative accuracy is best estimated by comparing the independently measured order parameter values.

These comparisons are done by several authors and generally they show a very good agreement [24–27, 53]. Botan et al. collected literature values for PC lipid choline headgroup and glycerol backbone order parameters and concluded that order parameters would be known with the accuracy of $\pm$0.02 for these segments in purified PC lipid bilayer samples [27] which agrees with the estimate of Gross et al [24]. Based on this Botan et al. suggested sweet spots where choline and glycerol backbone order parameters should fall in the simulation models, see Fig. 1 A). Also acyl chain order parameters from different techniques are in good agreement when compared by several authors [24–26, 53], however the 0.02 accuracy might not be achieved for some segments.**4.Maybe specify to which ones?**. The comparison by Ferreira et al. [26] for POPC acyl chains is also shown in Fig. 1 C).

Qualitative accuracy of experimental order parameter values

When order parameter changes are measured with varying conditions, like temperature [11, 13, 60], hydration level [25, 34, 54, 55], presense of ions [33, 56–58], cholesterol [26, 53, 59, 60] or proteins [52, 61, 62], the prefactors

connecting the order parameters and the measured couplings in Eqs. 2 and 3 can be considered to be unchanged. Therefore, accuracy of the measured change is determined by the accuracy of the splitting measurement in contrast to the prefactor in previous section. Here we refer to this as a qualitative accuracy. Due to the high resolution of splitting measurements, especially in ^{2}H NMR, the qualitative accuracy is much higher than the quantitative accuracy discussed in previous section.

The high qualitative accuracy of order parameter measurements is demonstrated in Figs. 2 and 3 showing the measured changes as a function of ion concetrations and hydration level, respectively. Systematically observed order parameter decrease of choline α and β segments due to penetrating positive charges [33, 56–58] from ^{2}H NMR are shown in Fig. 2 A). The quadrupole splittings reported in the original work [33] and corresponding order parameters are shown. The clearly measurable quadrupolar splitting changes correspond order parameter changes below 0.03 and 0.05 units for β and α, respectively. Systematically observed increase for choline β and α segments due to decreased hydration level is shown in Fig. 3. Similar increase is observed for different phosphatidycholine lipids in slightly different temperatures measured by different groups by using both ^{2}H NMR [34, 54] and ^{13}C NMR [70]. The results demonstrate the systematic changes only slightly above 0.01 units can be detected also with ^{13}C NMR [70].

In conclusion, the order parameter changes can be measured with very high accuracy, thus even very small structural changes can be observed. Molecular models are necessary to analyze the measured changes to avoid overinterpretation from tiny changes observed in experiments. For example, high concentration of cholesterol induces measurable changes (less than 2 kHz) to the DPPC α and β quadrupolar splittings, however, the related structural changes are probably almost negligible [27, 59].

Signs of order parameters

The ^{2}H NMR [23] and standard ^{1}H-^{13}C NMR [24–26, 28] techniques measure only the absolute value of order parameter. However, two different ^{1}H-^{13}C NMR techniques applied to eggPC [28] and DMPC [24, 28] allow also the measurement of the sign. The experiments report negative order parameters for almost all the segments, only α and γ are positive. Furthermore, the signs [17, 24, 28] and magnitudes [26, 27, 30] of choline headgroup and glycerol backbone order parameters are practically unaffected by the acyl tail contents of the bilayers. The results indicate that the order parameter signs for these segments can be assumed to be the same in all PC lipids in bilayer. On the other hand, the positive signs for g_1, g_3 and C_2 has been reported by Aussenac et al. [64] which has led to some confusion in simulation community [36, 71, 72]. However, these signs are not directly measured but extracted from the model used to interpret ^{2}H NMR order parameters from DMPC bicelles [64]. Thus, it is reasonable to conclude that order parameters are negative for all segments except for α and γ, as directly measured with ^{1}H-^{13}C NMR [17, 24, 28].

In the measurements of order parameter changes respect to varying conditions [11, 13, 25, 26, 33, 34, 52–62] only the absolute values are measured. However, the experiments are usually done by gradually changing the conditions and systematic order parameter responses are observed [26, 33, 34, 54–56, 70] (see also Figs. 2 and 3), indicating that sudden changes of sign are not present. On the other hand, large amount of bound positive charge may decrease the α carbon order parameter below zero as demonstrated by the spectra measured by Altenbach and Seelig [56] for POPC with high concetrations of $CaCl_2$, shown in Fig. 4.

Forking of order parameters

The order parameters for two C–H bonds in the same CH_2 segment are equal for the most segments in lipids [11, 13, 14, 24–26, 30]. However, this is not the case for g_1, g_3, and C_2 carbon in the *sn*-2 chain segments in a fluid PC lipid bilayer as observed with both ^{2}H NMR [14, 29–31] and ^{1}H-^{13}C NMR techniques [24–26], see also Fig. 1. We call this phenomena as *forking*, as done also previously to avoid confusion with splittings measured with NMR [27].

The forking has been studied in detail with ^{2}H NMR techniques by separately deuterating the R or S position in CH_2 segments to assign order parameters to correct hydrogens [30, 31]. These studies also show that the forking arises from differently sampled orientations of the two C–H bonds, not from two separate populations of lipid conformations [30, 31]. This means that the realistic atomistic resolution molecular model has to reproduce the forking correctly and the isomeric positions of hydrogens must be taken into account when calculating order parameters from simulations [27].

Order parameters from simulations

Since all the atom coordinates are available from molecular dynamics simulations trajectory, the order parameters can be calculated directly from the definition in Eq. 1. The ensemble average is taken over the time and all the molecules in simulation. The hydrogen positions can be generated post-simulationally for united atom simulations without explicit hydrogens by creating a trajectory with added hydrogens [27, 73], or by using equations to directly calculate order parameters [74, 75] based on heavy atoms positions and the known hydrocarbon geometries. The first approach necessary for accurate structural studies since it allows the analysis of forking in contrast to the latter.

The difference in the analysis methods for the forked segments is most likely reason for different choline and glycerol backbone order parameters reported for the same models by different authors [27, 76]. Also different order parameters for C–H segments attached to double bond are reported for the

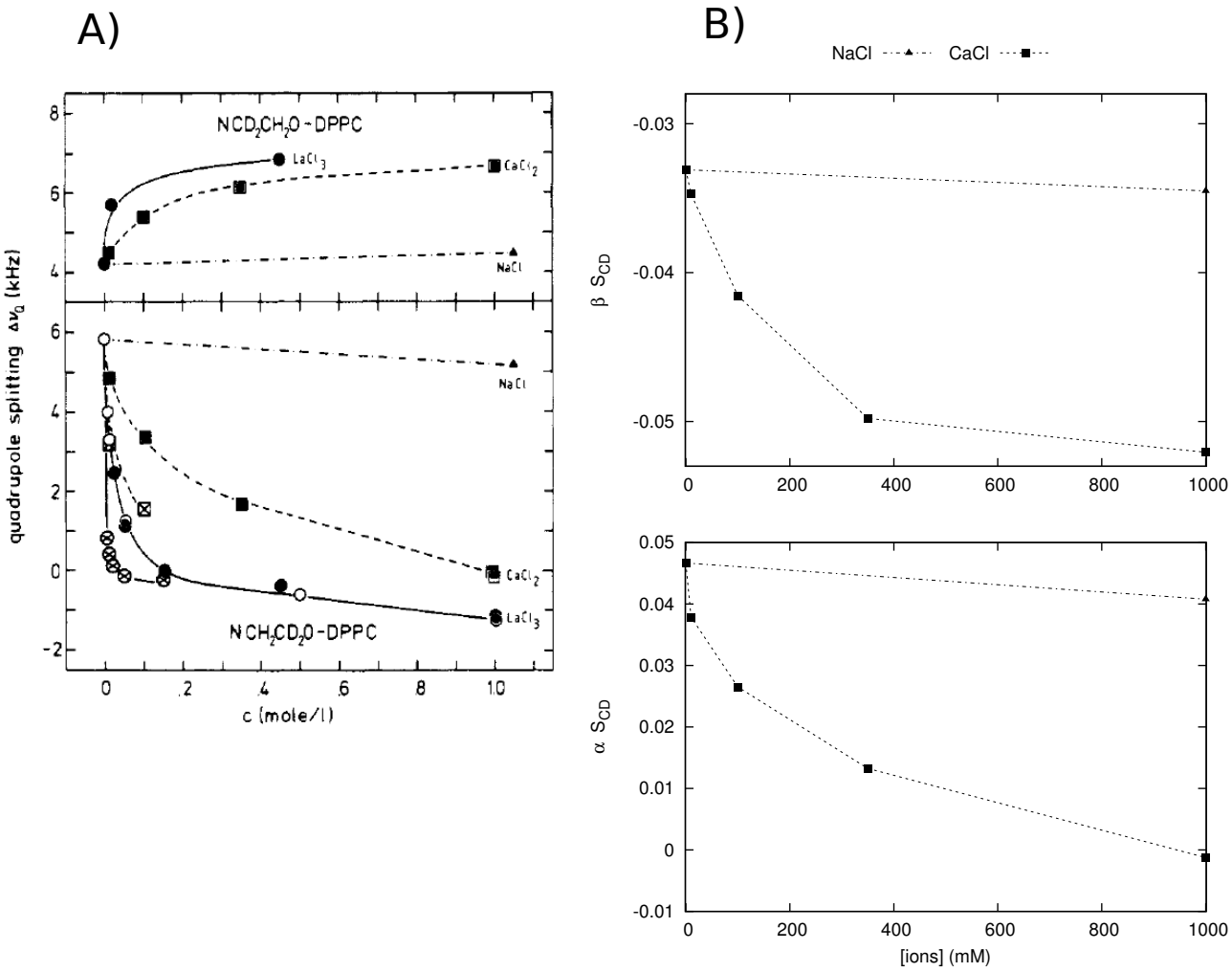

FIG. 2: A) Quadrupolar splittings of DPPC α and β segments as a function of different ion concetrations measured by Akutsu and Seelig with ^{2}H NMR [33]. B) The measured quadrupolar splittings with NaCl and $CaCl_2$ translated to order parameters ($S_{\rm CD} = 0.00784 \times \Delta\nu_{\rm Q}$). The negative sign for β order parameter is assigned according to more recent experiments [17, 24, 28] (see also Ref. [27] and Section 4). These changes were later shown to be consistent with the addition of different charges into the bilayer, and the electrometer concept was introduced to measure the amount of charge incorporated in the bilayer interface [33, 56–58].

same model [73, 77] due to bug in widely used version of *g_order* program in the Gromacs package. The *g_order* program also prints -$S_{\rm CH}$ which is most likely the reason to the reported positive order parameters for acyl chains in some studies [78]. When these technical issues are taken into account, the different order parameters calculations from simulations are in good agreement.

The statistical error for order parameters is estimated by using the error of the mean for time blocks [73], independent simulations [76] and different lipids [27]. All these approaches gives the maximum error bars of $\sim \pm 0.01$.

It was recently pointed out that the sampling of individual dihedral angles might be very slow compared to the typical (100 ns) simulation timescales [79]. This result raises a question if the molecules sample the full phase phase during typical simulation time scales. On the other, another recent study showed that the slowest rotational auto-correlation function observed (for g_1 segment) in the Berger model reached a plateau ($S^2_{\rm CH}$) after $\sim$200 ns and its relaxation was significantly too slow compared to NMR relaxation experiments [21]. This indicates that the typical simulation times are long enough for full conformational phase space sampling for the models with realistic dynamics [21].

Comparison between order parameters from simulations and experiments

The acyl chain order parameters are compared between simulations and experiments since the early days of lipid bilayer simulations [8, 35, 74, 80–89]. Good agreement has been generally found [19, 35–47]. except for C_2 segment in *sn-2* chain which has low magnitude and significant forking in all PC lipids, in constrast to C_2 in *sn*-1 [11, 24–26, 29],

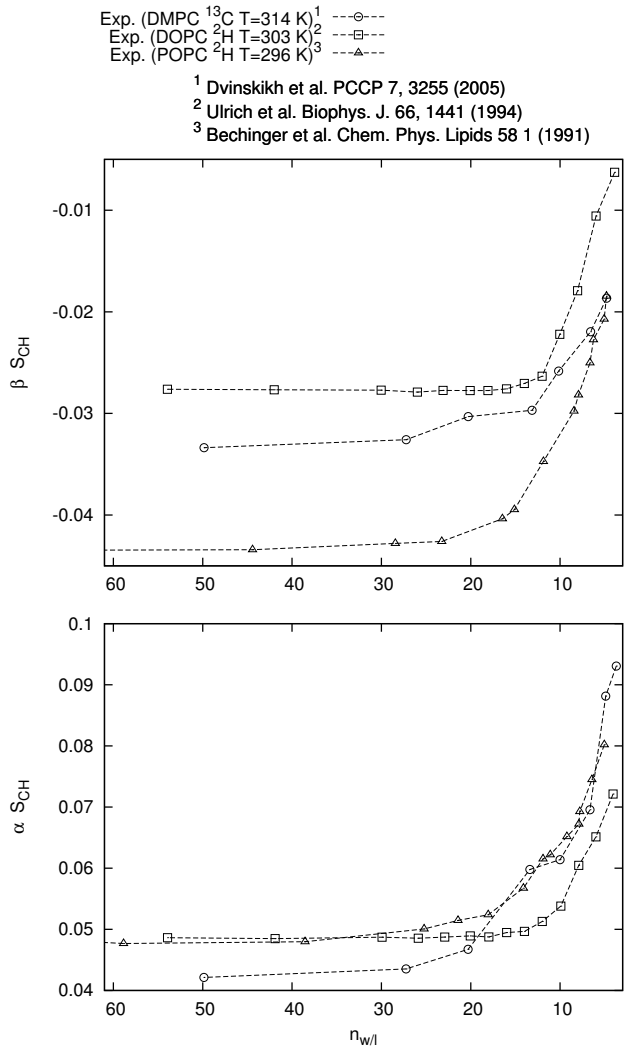

FIG. 3: Systematic increase of phosphatidylcholine α and β order parameters with decreasing hydration level, observed with both ^{2}H NMR [34, 54] and ^{13}C NMR [70]. The negative sign for β order parameter is assigned according to more recent experiments [17, 24, 28] (see also Ref. [27] and Section 4). The choline order parameter increase is related to the P-N vector tilting more parallel to the membrane plane [27] while relation between order parameter decrease and tilting more perpendicular has been suggested [58].

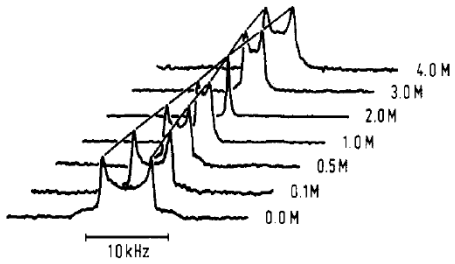

FIGURE 1: ^{2}H NMR spectra of coarse dispersions of POPC bilayers at various $CaCl_2$ concentrations (no NaCl). The lipid was deuterated at the α-segment ($-NCH_2CD_2OP-$). Measuring temperature, 40 °C.

FIG. 4: Quadrupolar splitting $\Delta\nu_Q$ for α segment in POPC as a function of $CaCl_2$ concentration measured by Altenbach and Seelig [56]. The splitting is related to the order parameter as $S_{\rm CD} = 0.00784 \times \Delta\nu_Q$. More recent studies show that the α order parameter is positive in the absense of $CaCl_2$ [17, 24, 28]. Thus, the most obvious interpertation is that the α order parameter decreases to zero when $CaCl_2$ concentration reaches 2.0M, and becomes increasingly negative with further addition of $CaCl_2$. Reprinted with permission from Altenbach and Seelig, Biochemistry, 23, 3913 (1984). Copyright 1984 American Chemical Society.

for example see Fig. 1 C). This feature is, however, not analyzed or not reproduced for several lipid models [19, 36, 38–40, 42–45, 90] while some models report the lower magnitude but the forking is not reproduced correctly or analyzed [19, 41, 46, 90]. The united atom CHARMM36 is really close the experimental results [47].

Also acyl chain order changes with varying conditions are compared between simulations and experiments by several authors. Experimentally observed order parameter increase with cholesterol concentration [26, 60, 75, 91–93] and dehydration [55, 70] is observed also in simulations [26, 71, 75, 94–98], as well as the temperature induced order parameter decrease [60, 99]. More careful comparison reveals, however, that the temperature and dehydration effects are slightly underestimated in simulations compared to experiments [71, 99]. Also cholesterol effect to DMPC bilayer is underestimated in CHARMM36 model [96], while Slipids [97] and Amber Lipid14 [98] models show satisfactory agreement. The comparison of Berger/Höltje [35, 100] based model to the extensive data set with various POPC/cholesterol mixtures shows a good agreement with experiments for low cholesterol concetrations, however, with 34% and higher cholesterol concentrations the agreement gets worse [26]. Recent comparison of the Amber Lipid14 model to the same data shows signifincantly better agreement [98] as also shown in Fig. 5. The orientation of cholesterol ring structure is reasonable in all models [26, 75, 96, 98], however, the cholesterol acyl chain has too low order parameters in Berger/Höltje [35, 100] based model and too much forking in Amber Lipid14 [98] while CHARMM36 reproduces experiments well [96].

The acyl chain order parameter decrease due to double bonds is generally reproduced by different simulation models [26, 41, 42, 46, 47, 73, 77, 97, 101–109]. Especially good agreement often achieved for oleyl chain in POPC bilayer with one *cis* double bond is demonstrated in Fig. 1 C). Also the further order parameter decrease due to multiple double bonds (polyunsaturation) [73, 77, 101, 102, 104–106, 108, 109] is usually well reproduced, as demonstrated in Fig. 6 for Berger [35] based model with double bond description by Bachar et al. [77]. Also difference between *cis* and *trans* double bonds can be reproduced in MD simulations

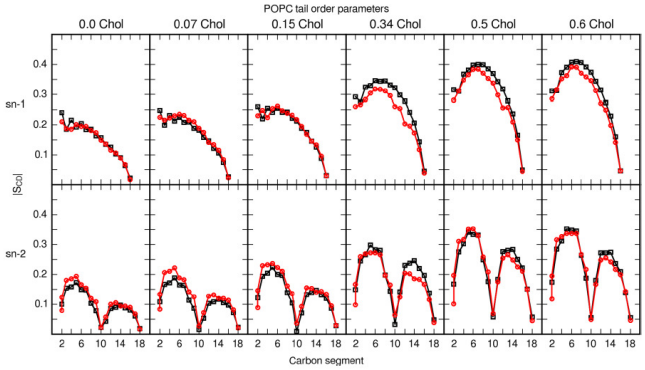

FIG. 5: Cholesterol effect on acyl chain order parameters compared between ? model [98] and experiments [26]. The agreement with experiments with this model is significanly better than Beger/Höltje based model compared by Ferreira et al. [26].

[110].

In contrast to acyl chains, the glycerol backbone and choline order parameters are not routinely compared between simulations and experiments. In most comparisons the experimentally available sings, stereospecific labeling and high accuracy are not fully exploited [27, 36, 41, 42, 71, 76, 88, 113]. These issues were recently dicussed by Botan et al. who also compared order parameters between 13 different simulation models and experiments [27]. The results, shown also in Fig. 1 A), reveal significant differences between models and experiments, and none of the available models reproduces all order parameters within experimental error. On the other hand, experimentally observed choline order parameter increase and decrease with dehydration [34, 54, 70] and cation penetration [33, 56], respectively, were reproduced in simulations [27, 63]. However, especially the effect induced by Na^+ ion penetration is strongly overestimated in most models which arises most likely from artificially high partition coefficient [63], as also demonstrated in Fig. 7. The effect of cholesterol on glycerol backbone and choline was overestimated by the Berger/Höltje based model while CHARMM36 and MacRog performed better [27].

In conclusion, the acyl chain order parameters and their qualitative changes are generally well described in atomistic MD models, except for C_2 segment in *sn*-2. However, all models have difficulties with varying severity to describe the glycerol backbone and choline order parameters.

Interplay between simulations and NMR order parameters: Validation and interpretation

Since the acyl chain order parameters from MD models generally agree with experiments for single component lipid bilayers in full hydration, the conformations sampled in simulations can be considered as realistic atomistic resolution structures for the acyl chains (except for the C_2 segment in the *sn*-2 chain). As also the acyl chain rotational dynamics has correct order of magnitude (see Section 4), the dynamical nature of hydrophopic region of lipid bilayers seen in simulation videos can be considered as a realistic representation. This is significant advancement to the traditional static structural models [11, 14, 16, 114]. Since lipid bilayers are considered as a simple models for cell- and other biological membranes, the intuitive understanding of their dynamical nature has a significant impact on biomembrane physics and chemistry.

Also more detailed structural interpretation has been succesfull for acyl chain region, especially for order parameter decrease due to *cis* double bonds [73, 77, 105, 106, 115–117]. From NMR experiments alone it was not possible to judge if the order parameter decrease arises from reduced chain order or the changes in average θ angle in Eq. 1 [116**?** , 117]. The interpretation of NMR experiments with the help of MD simulations and other calculations revealed that double bonds, indeed, decrease the chain order due to the flexible dihedral potentials next to the rigid double bonds [73, 77, 105, 106, 115–117].

The acyl chain order parameter increase and related bilayer thickening with cholesterol concentration [26, 98**?**], dehydration [71, 94] and reduced temperature [99] are qualitatively reproduced by simulations giving intuitive visualizations for these effects. However, the order parameter changes are often under- or overestimated [26, 71, 96, 98**?** , 99], thus it is not clear how well the models can be used for atomistic resolution intepretation of these changes. For example, delicate lipid-cholesterol interactions are known to induce liquid-ordereded and liquid-disordered phase coexistence [118]. To give atomistic resolution interpreation for this phenomena, the atomistic resolution structures and interactions should be correct, which does not seem to the case for Berger/Höltje based model [26] while recent Amber Lipid14 model performs better [98].

Simulation studies have also predicted changes in the acyl chain region which are yet to be experimentally confirmed, e.g. order parameter decrease due to lipid oxidation and changes in order parameter sign in oxidized acyl chain [78].

The usability of MD models for structural interpretation decreases close to the interfacial region since experimental glycerol backbone, choline headgroup and *sn*-2 C_2 segment

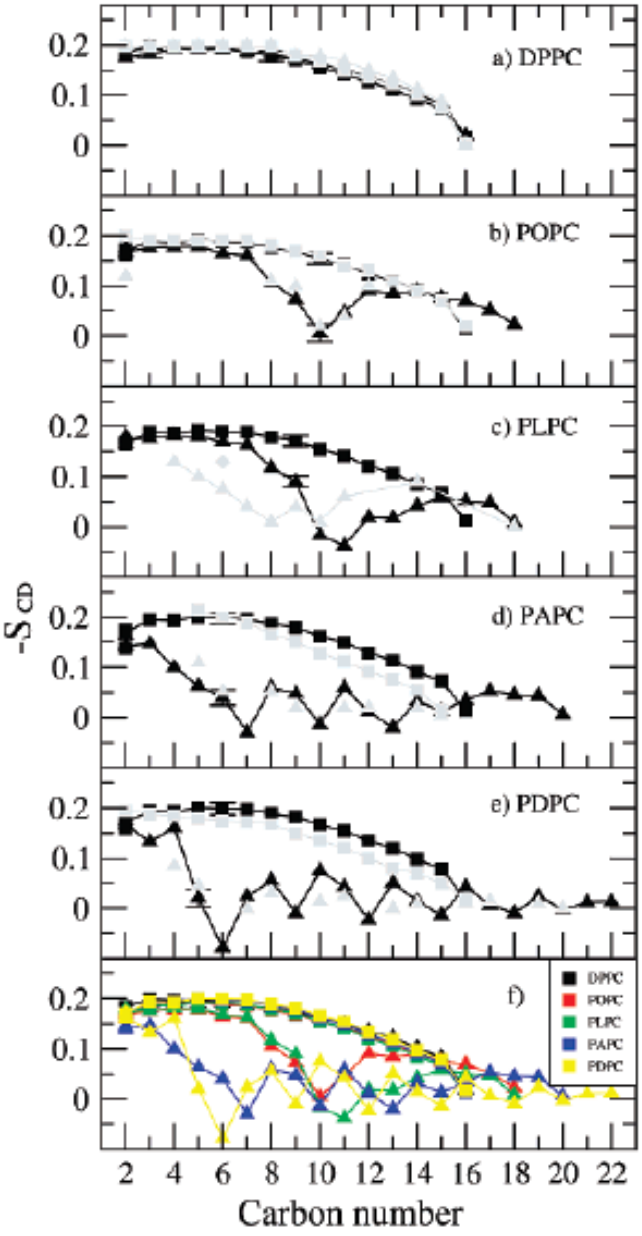

FIG. 6: Figure comparing order parameters in polyunsaturated acyl chains between simulations and experiments adapted from [73]. Order parameters for the sn-1 (squares) and sn-2 (triangles) chains of (A) DPPC, (B) POPC, (C) PLPC, (D) PAPC, and (E) PDPC. Simulation results are shown in full black, and experimental results for comparison in gray. Additionally, part F summarizes the data for all bilayers from the simulations. Experimental order parameters were chosen for comparison as follows. The order parameters for DPPC (T=323K) are based on studies by Petrache et al. [111] whereas the experimental S_{CD} values for PDPC and for the sn-1 chain of POPC (T=310 K) are based on studies by Huber et al. [105] For the sn-1 chain of PDPC, the data set at 310 K is obtained by linearly interpolating between data at 303 and 323 K, whereas for the sn-2 chain the data at 303 K are presented [105]. Experimental values for the sn-2 chain of POPC are based on studies by Seelig et al. [14] A single experimental value is available also for the sn-2 chain of the PLPC bilayer at 313 K (diamond) [16] to compare with our simulated order parameters for PLPC. Together with PLPC, there are also experimental results for PiLPC (T=313K) [16]. Experimental order parameters for the sn-1 and sn-2 chains of PAPC (T=303 K) are based on quadrupole splittings measured by Rajamoorthi et al. [112]. For the sn-1 chain the monotonic decrease through the acyl chain is expected. For the sn-2 chain, values are fitted such that the agreement is as good as possible.

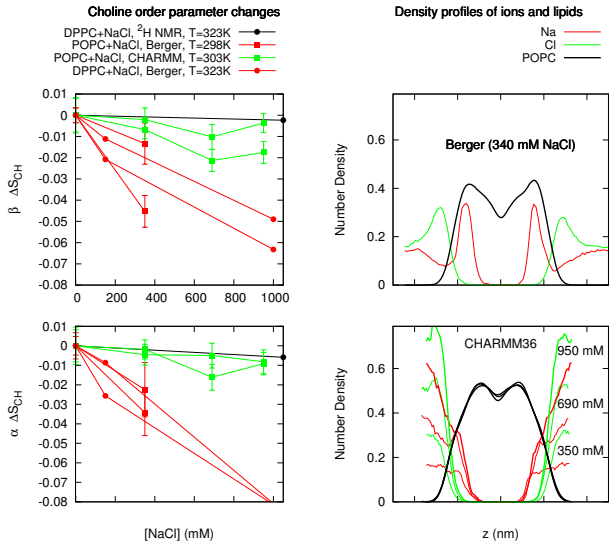

FIG. 7: Changes in choline order parameters (left column) and ion density distributions (right column) as a function of NaCl concentration. Significant order parameter reduction and Na^+ partition is observed with Berger model while only modest order parameter change and ion parition observed with CHARMM36. The results are in line with the electrometer concept connecting the ion partition and choline order parameters changes [33, 56–58]. Consequently, the results show that Na^+ partition is significantly overestimated in the Berger model. For more discussion see [63].

order parameters are not usually reproduced within experimental error. The forking and low order parameter values for C_2 in the *sn*-2 are related to the parallel orientation of the chain respect to membrane normal [29, 114] which is suggested to have significant contribution e.g. to membrane electrostatic potential [119]. Also the atomistic resolution structures sampled by glycerol backbone and choline headgroup are not yet fully resolved [12, 13, 15, 18, 120, 121]. Unfortunately the accuracy of atomistic resolution models is not yet sufficient to solve these issues. However, the modeling of interfacial region structure has been getting more attention lately [19, 20, 27, 41, 42], thus higher quality models may be expected.

On the other hand, the increase of choline α and β order parameters with dehydration and decrease with cation penetration were correctly reproduced by several models, despite of inaccurate choline structures [27, 63]. The order parameter increase was related to the choline P–N vector tilting more parallel to the membrane normal [27] and order parameter decrease to the cation binding affinity [63]. The observations are in line with previous studies on charge penetration [33, 56–58]. However, choline structural changes due to cholesterol or ion concentration are significantly overestimated in several models [26, 27, 63, 98], especially Na^+ binding affinity [63] (see also Fig. 7). The artificial specific Na^+ binding induces effectively postively charged membrane which may

easily lead to errorneous conclusion due to dominant contribution of electrostatics for various phenomena.

In conclusion, the atomistic resolution MD simulations are invaluable in understanding the structural details and their changes in acyl chain region. However, in applications where lipid interfacial region structure, energetics, electrostatics or ion distributions have significant role, the potential artefacts arising from simulation models must be cafefully taken into account. A typical example of such application would be a study of interactions between charge containing protein in solution and lipid bilayer, simulated in physiological salt concentration [122, 123].

C-H BOND ROTATIONAL DYNAMICS FROM SPIN RELAXATION RATES AND SIMULATIONS

5.This is the first sketch of this section. A lot of references should be added, the text should polished, things should be added and checked and figures should be improved. However, the main strucutre and idea of the section should be visible.

Definition and properties of rotational autcorrelation function

The second order auto-correlation function for the reorientation of the C–H chemical bond axis is defined as [124]

$$g(\tau) = \langle P_2[\vec{\mu}(t) \cdot \vec{\mu}(t+\tau)]\rangle, \tag{4}$$

where P_2 denotes the second Legendre polynomial, $P_2(\xi) = 1/2(3\xi^2 - 1)$, $\vec{\mu}(t)$ is the unitary vector having the direction of the C–H bond at time t, and the angular brackets denote a time-average. This autocorrelation is usually chosen to describe the C–H bond rotational dynamics since it is connected to the experimentally measurable spin relaxation rates through its Fourier transformation called spectral density

$$j(\omega) = 2\int_0^\infty \cos(\omega\tau)g(\tau)d\tau. \tag{5}$$

In this review we focus only on experiments measured from multilamellar samples with randomly oriented sheets, thus only the second order auto-correlation function is needed [**?**].

In randomly oriented multilamellar samples the auto–correlation function of bond orientations always decays to zero with long enough time scales. However, the relaxation timescales can be divided to two distinct timescales. First the relaxation processes shorter than microsecond timescales occurs when lipid molecules are reorienting in the lipid bilyer but are not essentially moving between lipid bilayer regions with different orientations. Then with larger than microsecond timescales the movement between differently oriented bilayer regions decays the rotational correlation function to zero. In addition, MAS experiments the sample spinning causes lead orientaitional relaxation in kHz region. The full auto–correlation decaying to zero is illustrated in Fig. 8. Due to the timescale separation the correlation function can be written as [125]

$$g(\tau) = g_\mathrm{f}(\tau)g_\mathrm{s}(\tau); \tag{6}$$

$g_\mathrm{f}(\tau)$ describes the decay of $g(\tau)$ due to fast molecular motions and $g_\mathrm{s}(\tau)$ contains the contribution from slower motions

$$g_\mathrm{s}(\tau) = e^{-\frac{\tau}{\tau_\mathrm{s}}}\left[\frac{2}{3}\cos(\omega_R\tau) + \frac{1}{3}\cos(2\omega_R\tau)\right], \tag{7}$$

where τ_s is a correlation time due to slower isotropic molecular motions originating from the diffusion between bilayers with different orientations of their principal symmetry axis, and the cosine terms are the contribution from magic angle spinning of the sample, rotating at $\omega_\mathrm{R}/2\pi$ cycles per second [126], typically in the kHz frequency range.

The order parameter measurements with ^{2}H NMR and ^{13}C NMR measure the bond order after the relaxation of rotational motion inside the bilayer plane but before the relaxation between different bilayer orientations, as illustrated in Fig. 8. In typical molecular dynamics simulations with periodic boundary conditions the lipid molecules are restricted to single bilayer orientation and also the timescales are currently typically below microsecond. In these simulations the auto–correlation function in Eq. 4 decays to the square of order parameter in Eg. 1 in bilayers with planar symmetry, i.e. no microscopic phase separation of defects present. Also this is illustrated in Fig. 8.

The rotational correlation function describes how long does it take for a single molecule on average to sample the conformations. The effective correlation time

$$\tau_e := \int_0^\infty \frac{g_\mathrm{f}(\tau) - S^2_\mathrm{CH}}{1 - S^2_\mathrm{CH}}\mathrm{d}\tau \tag{8}$$

can be used as an intuitively useful single parameter to describe this time. The larger this parameter is, the longer it takes in average to sample the conformations related to the bond. With this definition the area between the correlation function and its pleateau becomes $(1 - S^2_\mathrm{CH})\tau_e$.

Detecting C–H bond dynamics experimentally

The most used parameter to detect the C–H bond dynamics experimentally in time scales comparable to simulations are the spin-lattice relaxation rates R_1 from deuterium labels and ^{13}C. R_1^C measured from ^{13}C is connected to the spectral density (Eq. 5) through the equation

$$R_1^C = \frac{D^2_\mathrm{max}N_\mathrm{H}}{20}\left[j(\omega_\mathrm{H}-\omega_\mathrm{C})+3j(\omega_\mathrm{C})+6j(\omega_\mathrm{C}+\omega_\mathrm{H})\right], \tag{9}$$

where ω_C and ω_H are the Larmor angular frequencies of ^{13}C and ^{1}H respectively, N_H is the number of bound protons and $\frac{D_\mathrm{max}}{2\pi}$ ≈22 kHz as in section 2. R_1^D measured from ^{2}H is

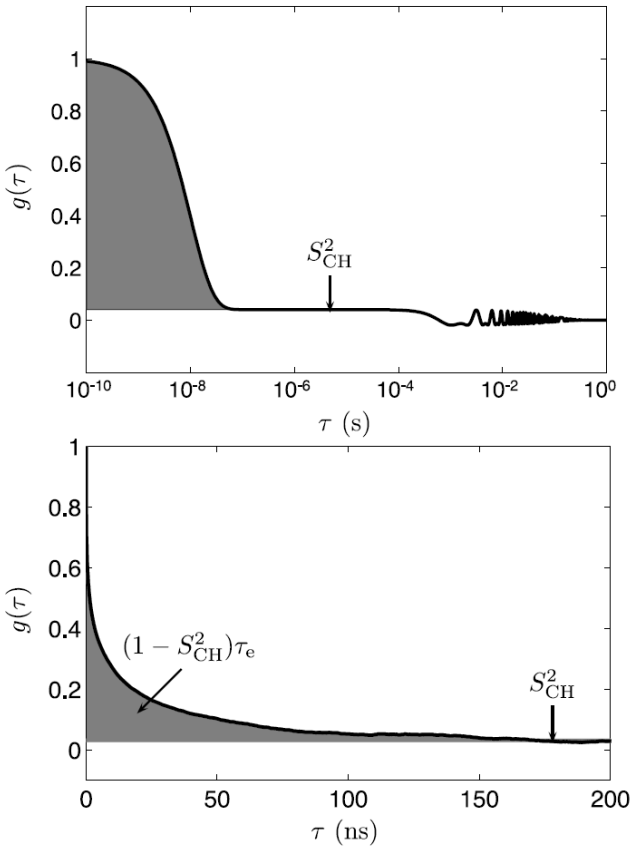

FIG. 8: (Top) Illustration of the auto-correlation function $g(\tau)$ and effective correlation time τ_e for a 13CH bond in a lipid bilayer in MAS experiment (x–axis with logarithmic scale). Plateau after short timescale relaxation processes $(g(\tau)_f)$ is shown between roughly 10^{-7}s and 10^{-4}s. After this timescale the slow relaxation processes $(g(\tau)_f)$ and oscillation due to MAS (Eq. 7) are shown. (Bottom) Example of $g(\tau)$ from a united-atom MD simulation of a POPC bilayer in excess water, illustrating the decay towards $S^2_{\rm CH}$ (x–axis with linear scale). This represents the $g(\tau)_f$ in Eq. 6 and decrease to the plateau in the top figure. The effective correlation time τ_e is equal to the area in gray scaled by $(1S^2_{\rm CH})^1$. Figure adapted from [21]

connected to the spectral density (Eq. 5) through the equation

$$R_1^D = \frac{12\pi^2}{40}\left(\frac{e^2qQ}{h}\right)^2\Big[j(\omega_{\rm D}) + 4j(2\omega_{\rm D})\Big], \qquad (10)$$

where $\frac{e^2qQ}{h}$=170kHz as in the case of order parameters in section 2.

Also the model free approach to measure the effective correlation time (Eq. 8) was recently introduced [21]. The method is based on the combination of experimental order parameter $S_{\rm CH}$, spin-lattice relaxation rates R_1 and the transverse magnetization under a spin lock pulse $R_{1\rho}$ with measured appropriate nutation frequency through equation

$$\tau_{\rm e} \approx \frac{5R_{1\rho}^{\rm plateau} - 3.82R_1^C}{D^2_{\rm max}N_{\rm H}(1-S^2_{\rm CH})}. \qquad (11)$$

Analyzing C–H bond dynamics from simulations

As in the case of order parameters, the auto–correlation function for each C–H bond can be calculated directly from simulations using the definition in Eq. 4 since the trajectories of each atom is known as a function of time. As in the case of order parameters the positions of hydrogens can be determined for united atom models based on heavy atom positions and assuming tetrahedral configurations [21, 127, 128]. Usually in the correlation function calculation all the available time intervals from the simulation data are used and the average over those and all molecules is taken. However, since the amount of data decreases when the the time interval approaches the total length of the simulation, usually the largest time interval used is the half of the total simulation length, for more details see [129].

To connect the auto–correltaion functions from simulations to the experimentally measurable spin lattice relaxation times, the spectral density (Eq. 5) must be first calculated. In principle, this could be done using numerical fourier transformations techniques, however this often leads to unneccessarily large fluctuations. Instead, commonly used apporach is to fit analytical functional form to the calculated auto–correlation function and then use analytical Fourier transform of the fitted function [9, 21, 127, 128, 130]. Most commonly the sum of 4 or more exponentials is used as a fitting function [9, 21, 73, 115, 130, 131] but also streched exponential has been used [127, 128]. Numerically the functional form of the fitting function should not matter as long as the fit is good, however, theoretically the correct correlation function form to describe the modes of physical motion can be debated [50, 128, 132–134]. It is clear from correlation functions from simulations that one exponential is not enought to produce a good fit while 4 gives a reasonable fit [115]. This is not surprising since more than one relaxation timescale is definitiely expected to be present in lipids in bilayer [9, 50, 130, 131].

After the fitting the analytical form of the spectral density predicted by simulations is available. Then its values can be calculated at the required larmor frequency values and substituted to Eqs. 9 and 10 to get the R_1^C and R_1^D. The value of the effective correlation time can be calculated directly from the interated area below the correlation function, see Fig. 8 or from Eq. 30 in Ref. [21].

Comparing C–H bond dynamcis between simulations and NMR experiments

The spin lattice relaxation parameters R_1^C, R_1^D and $R_{1\rho}$ are considered as directly measurable experimental parameters and the effective correlation time τ_e can be derived directly from directly measurable parameters without further assumptions (see Eq. 11 and Ref. [21]). Spin lattice relaxation parameters R_1^C and R_1^D can be calculated from simulations by first calculating the auto–correlation function (Eq. 4), then calculating the spectral density from the Fourier transformation (Eq. 5) and finally substituting its values into Eqs. 9 and 10 (see also previous section). The effective correlation time can be calculated directly from integrated area and order parameter or from Eq. 30 in Ref. [21]. In practise, the $R_{1\rho}$ cannot be calculated from simulations directly since its value depends also on the slow relaxation dynamics ($g_s(t)$ in Eq. 6) which is not present in simulations. The same applies to the calculation of NOESY relaxations rates and in this case decay time of 170 ns was assumed for the $g_s(t)$ [135], while 4.2 ms was measured by Ferreira et al. [21].

As seen from Eqs. 9 and 10, the numerical values of R_1^C and R_1^D depend also on the carbon ω_C, hydrogen ω_H and deuterium ω_D Larmor frequencies which, in turn, depend on the spectrometer external magnetic field. From simulations it is straighforwad to calculate the spectral density with any Larmor frequncy value to get the R_1^C and R_1^D as a function of external magnetic field. However, in experiments with standard spectrometers the external field cannot be changed, i.e. each spectrometer has their specific field strengths. Thus, to measure R_1^C or R_1^D values as a function of magnetic field one has to use several spectrometers which is tedious and spectrometers excists only with limited amount of magnetic field strengths. Despite of these challenges this kind of experiments have been done and the available data is reviewed by Leftin et al. [50]. Another approach to measure the magnetic field strength depedence of spin lattice relaxation times is the Field Cycling NMR [136, 137]. However, this is not yet feasible with standard spectrometer and only limited amount of data is available, mostly from ^{31}P NMR [136–138] but also from ^{13}C NMR [69].

The magnetic field strength dependence of spin relaxation times between simulations and experiments is compared in several studies [9, 89, 127, 128, 130, 133]. Examples of such comparison for acyl chain segments are shown in Fig. 9. On the other, some studies have compared R_1^C and R_1^D measured with one magnetic field strenght to the value calculated from simulations [21, 73, 89, 106, 109, 115]. Example of such comparison between R_1^C from simulations and experiments is shown in Fig. 10 Comparisons seems to generally show a good agreement with large larmor frequencies which is getting worse when the Larmor frequency decreases. On the other hand, the level of the agreement depends on the carbon segment and the type of relaxation used in the comparison; Berger model compared with 2H NMR gives better agreement for C_7 segment compared to C_3 (Fig. 9 B)) while comparison

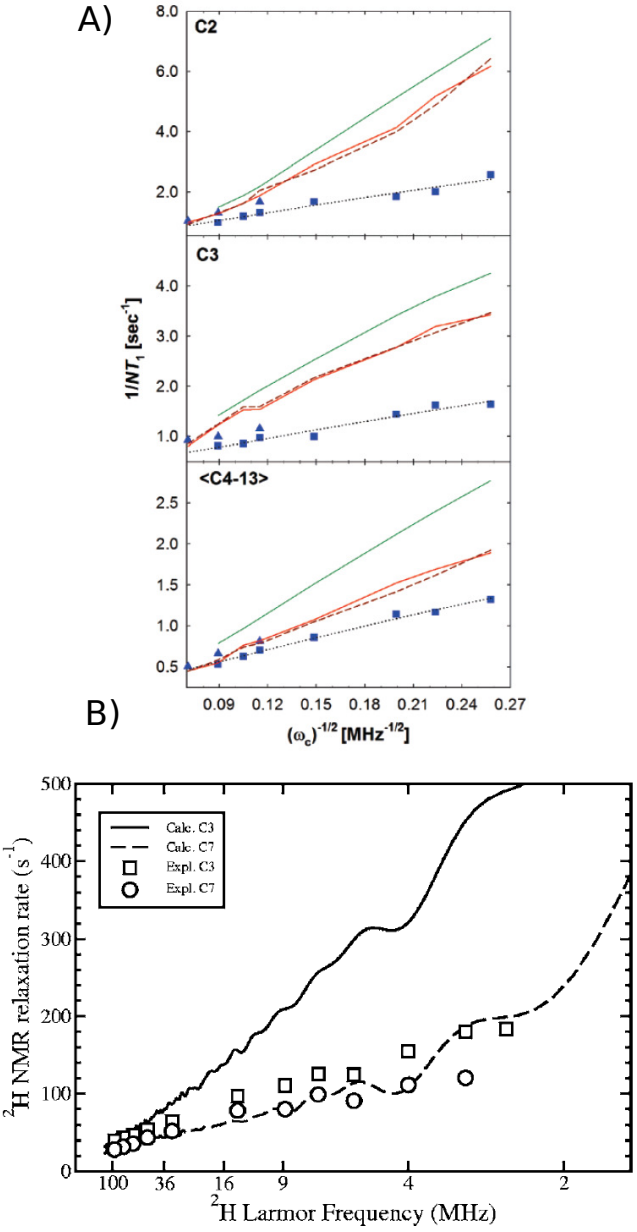

FIG. 9: A) Comparison of R_1^C dependence on magnetic field between experiments and CHARMM simulations for acyl chain carbons (DPPC bilayer in 323K) adapted from [133]. Experiments as points; MD simulations as solid and dashed lines; and a model-free fit to the vesicle data as dotted lines. B) Comparison of R_1^D dependence on magnetic field between experiments and Berger simulations for acyl chain carbons (DMPC bilayer in 300K) adapted from [128].

to 13C NMR relaxation with one frequency gives similar discrepancy for both segments (Fig. 10). For CHARMM the agreement seems better when going towards bilayer center, see Fig. 9 A). Due to the complicated connection between molecular dynamics and spin relaxation it is not straightforward to make conclusions about the dynamical differences between reality and simulations. This is, however, possible with

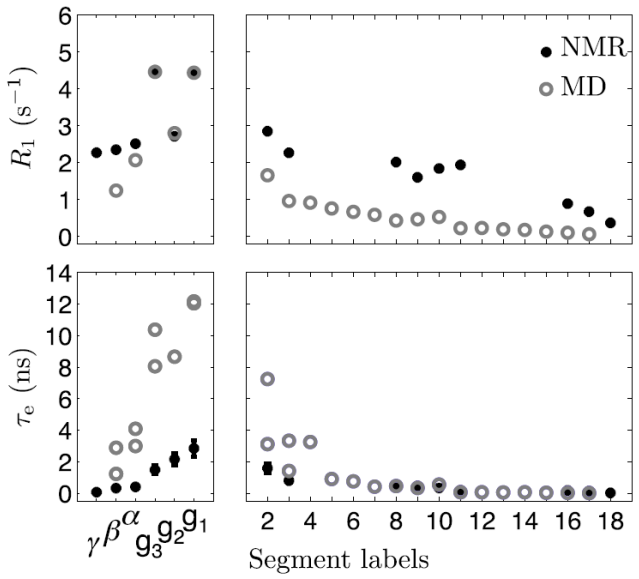

FIG. 10: (top) R_1^C for POPC bilayer in 298K calculated from simulations with Berger model compared to experimental results measured with field strength correspondin to the Larmor frequency of 125 MHz for ^{13}C. (bottom) Effective correlation times for the same system compared between simulations and experiments. Figure adapted from Ferreira et al. [21].

careful analysis as discussed in the next section.

To ease the intuitive interpretation of experimentally measured rotational dynamics Ferreira et al. showed that the effective correlation time can be measured by combining directly measurable quantities without any assumptions on dynamical prosesses present in the fast relaxation regime [21]. The comparison of effective correlation times between experiments and simulations for different segments is shown in Fig. 10. From this result it is straightforward to conclude that acyl chain rotational dynamics is generally well described while in the interfacial region, especially in glycerol backbone, the dynamics is too slow in simulations. It should be noted, however, that the effective correlation describes the total relaxation over all short timescales present in $g_f(t)$. Even if this is correct, the balance between different processes with different relaxatio times may not be correct. This is actually seen in the acyl chains, where R_1 does not perfectly agree with experiments while τ_e does.

Interplay between simulations and NMR spin lattice relaxation times: Validation and interpretation of dynamics

By measuring single spin relaxation time values it is almost impossible to make any conclusions about molecular dynamics due to their complicated connection through the spectral density. Even changes of relaxation times cannot be directly related to molecular dynamics without further information since, e.g. faster dynamics may lead to the decrease or increase of spin relaxation times, depending on the other dynamics processes present and the used magnetic field strength as demonstrated, for example in [21].

Careful studies of spin relaxation times as a function of temperature and magnetic field to overcome this issue are recently reviewed by Leftin and Brown [50]. From compilation of different experimental data sets it was possible to conclude, for example, that the interfacial region of lipid molecules has slower dynamics than acyl chains [50]. Another successfull approach to interpret the spin relaxation times has been to use the atomistic resolution molecular dynamics simulations to reproduce the measured changes and then analyze the dynamical changes from the simulation trajectory [106, 115, 139]. This approach has been especially useful in the studies of polyunsaturated acyl chain dynamics which concluded by combining the simulation and NMR relaxation data that the double bonds speed us the chain dynamics due to flexible dihedrals next to the double bonds [106, 115–117].

To ease the interpretation of the measured spin relaxation times Ferreira et al. recently introduced a model free connection between effective correlation time and directly measurable spin relaxation rates [21]. The main advantages of effective correlation time is that its connection to molecular dynamics is straightforward in the sense that the general dynamics is faster when effective correlation time decreases and *vice versa* and that it can be quantitatively compared to simulations. As shown in Fig. 10 these experiments immediately show that the glycerol backbone has the slowest dynamics of lipid segments (in agreement with conclusions from the combination of several previous experimental sets [50]) and that the dynamics of these is significantly underestimated by the Berger model.

Most importantly, the rough agreement of spin relaxation rates and effective correlation times between simulations and experiments shows that the rotational dynamical processes present in simulations has the correct order of magnitude [9, 21, 73, 89, 89, 106, 109, 115, 127, 128, 130, 133]. Consequently, the dynamical visualizations of simulation trajectories (videos) can be considered as a realistic intuitive presentations of lipid bilayers. However, in more detailed studies it should be kept in mind that all the dynamical (and also structural) details are not exactly correct.

The lipid rotational dynamics has been often interpreted by using the so called wobble in the cone model [9, 69, 130, 133, 134]. The main idea of the model is that the whole lipid molecule is wobbling as a cone such that all the all the segments share the time scale for this wobbling. In addition, each segments have further timescales related to their dynamincs inside the cone. The auto–correlation functions assuming the wobble in the cone model can be nicely fit to the simulation data and also some experimental results can be reproduced. However, also auto–correlation functions having different type of dynamics can be used to do the same. On the other hand, it has been recently pointed out that significant changes of structure and dynamics experienced in acyl

chain region may not reflect to the headgroup [27, 140] indicating weak coupling between these segments. This idea is also in line with one possible interpretation of recent field cycling experiments [138]. In addition, the role of undulations in the relaxation data measured with low frequencies is under discussion [50, 132–134].

In conclusion, the timescale of rotational dynamics is correct in simulations while the exact correlation times and relaxation processes are not fully reproduced. More experimental and simulation studies are needed to fully understand current quality of dynamics in current models. To interpretate the relaxation prcosesses present in lipid bilayer, a model which can be shown to agree with experiments on all fast timescales is needed.

STUCTURE FACTORS FROM SCATTERING AND SIMULATIONS

For this section I would be more than happy for some help

Form factor measured with X-ray or Neutron scattering

In scattering experiments the scattering intensity $I(q) \sim |F(q)|^2 S(q)$ is observed, where $F(q)$ is the form factor and $S(q)$ is the structure factor. In the case of lipid bilayer the structure factor describes the structure of lamellar sheets and the form factor describes the internal structure of lipid bilayers. The structure factor depends on the topological phase of lipids and can be considered to be practically constant for unilamellar vesicles while in multilamellar phase its form is known. Thus, in practise direct information about form factor is achieved from the measured scattering intensity.

Following the notation from Ref. [22], the form factor can be written as

$$|F(q)| = |\int_{-D/2}^{D/2} (\sum_{\alpha} f_\alpha(q_z) n_\alpha(z) - \rho_s)(\cos(zq_z) + i\sin(zq_z))\mathrm{d}z|, \tag{12}$$

where $n_\alpha(z)$ in the atom α number density as a function of membrane normal coordinate z, $f_\alpha(q_z)$ is the scattering length density, ρ_s is the solvent scattering lenght density and integral spans over bilayer with total thickness D. Neutron scattering length density or X-ray atomic form factors are used for $f_\alpha(q_z)$ depending on the used scattering technique. The values for these are available in the literature [**?**]. The last term disappears for symmetric bilayer but not for asymmetric [**?**]. If bilayer symmetry and delta functions for electron densities around atom center are assumed, the Eq. 12 becomes to the commonly used form for x-ray scattering

$$|F(q)| = |\int_{-D/2}^{D/2} \Delta\rho_e(z) \cos(zq_z)\mathrm{d}z|, \tag{13}$$

where $\Delta\rho_e(z)$ is the difference between solvent and the total electron densities.

The form factor can be measured from unilamellar vesicles, multilamellar vesicles or from order bilayer samples. The results from samples with different topologies are in good agreement, indicating that the bilayer structure is similar independently of the lamellar phase topology [141, 142]. Different sample topologies gives the highest resoution with different q ranges, thus the combination of form factors measured from different topologies are of the used to maximize the available form factor information [141]. In addition, the neutron scattering resolution is highest with small q values this giving more accurate on longer scales in real spave, like on bilayer thickness [**?**]. On the other hand, x-ray scattering has larger resolution with larger q values thus giving more accurate information on fine details of the bilayer density profile. Consequently, the neutron and x-ray scattering measurements complement each others and the combining the information from both gives the most comprehensible picture on bilayer strucuture [143].

Form factors are quite accurate given that experimental care has been taken. A delicate issue can be subtraction of background (from water and capillary).

6.Discussion about related issues can be found at: https://github.com/NMRLipids/NMRLipids_V-Review/issues/1

7.The discussion is going in at:

https://github.com/NMRLipids/NMRLipids_V-Review/issues/2

Key questions now:

Do we get independetly measured Form Factors plotted to the same figure?

Are there good references for the accuracy?

Form factor calculation from simulations

To calculate the scattering form factors from simulations the number density from simulations can be substituted into Eq. 12. In the case of neutrons the scattering length densities $f_\alpha(q_z)$ are assumed not to depend on q and numerical are usually taken from [**?**]. For x-ray scattering it is often assumed that all electrons pointwisely located in the atom position in simulation [**?**]. Also in most simulations the bilayer is symmetric, thus the electron density is simply calculated and substituted into Eq. 13. On the other hand, in some studies gaussian distribution for electrons around atom positions [144] or analytical expression for atom scattering length density $f_\alpha(q_z) = \sum_{j=1}^{4} a_j e^{-b_j(q/4\pi)^2} + c$ are assumed [22, 144**?**]. In the case of the analytical expression the parameters a_j, b_j and c are taken from [**?**]. For example, the widely used SIMtoEXP software is using the analytical form [22]. The effect of these choises on electron density profiles was discussed by

Benz et al. [144], however, it is not clear how significant this is when form factors are compared between simulations and experiments.

The small bilayer patches used in simulations might depress bilayer undulation modes which are present in large scale experiments [145]. Braun et al. showed that undulations seen in large enough simulations do not change the locations of form factor minimaz but depress the peak hights in the lobes [145]. Since the undulations are expected to be present in the experiments, the potential discrepancies between simulations and experiments in the lobe heights may be explained by the lack of undulation motions in experiments.

The simulations give the form factors on absolute scale while experiments obtain them only on relative scale, thus the experimental form factors from different sources has to be scaled for comparison [22, 143]. In SIMtoEXP program the scaling is performed using the scaling factor k determined from equation

$$k = \frac{\sum_{i=1}^{N} \frac{|F_s(q_i)||F_e(q_i)|}{(\Delta F_e(q_i))^2}}{\sum_{i=1}^{N} \frac{|F_e(q_i)|^2}{(\Delta F_e(q_i))^2}}, \quad (14)$$

where $F_e(q)$ and $F_s(q)$ are experimental and simulated form factors, respectively, $\Delta F_e(q)$ is the uncertainty of the experimental form factor and the summation goes over all N data points [22, 143]. In many studies which compare the form factors between experiments and simulations, the details on the scaling factor used is not given [**?**].

8.More discussion at:

https://github.com/NMRLipids/NMRLipids_V-Review/issues/3

and

https://github.com/NMRLipids/NMRLipids_V-Review/issues/4

I still think that I have seen undulation correction for experimental data mentioned in the literature.

Interplay between simulations and scattering experiments: Validation and interpretation

Similarly to NMR order parameters, the form factor gives accurate information about lipid bilayer structure but the structure cannot be uniquely resolved from the experimental data only. To give structural intepretation of order parameters, the model for sampled conformations of single molecules are needed while to interpret the scattering form factor data the model for the atom number densities, $n_\alpha(z)$ in Eq. 12, is needed. Several models developed and used for this purpose are reviewed by Heberle et al. [146].

Similarly to the NMR order parameters, also MD simulations can be used in the structural interpretation if they reproduce the experimental form factors. And in turn, if simulation model do not reproduce the experimental form factor its structure is not realistic. The comparison between experimental and simulated form factors has been done in several studies for both purposes, to validate the simulations model [19, 36, 40–47, 96–98, 109, 110] and to intepret the experiments [143, 147–150]. The simulations have been also used to improve the fitting based structural models [**?**].

The comparison to experimental area per molecule values to validate the lipid density simulations [74] has been often replaced nowdays with more direct comparison [5] using x-ray form factors [19, 36, 40–47, 96–98, 109, 110]. In some studies the comparison is complemented with the comparison to the neutron scattering data [42, 43, 45–47, 98] In general the models reproduce form factors in good agreement with experiments, especially with lower q values indicating that the bilayer dimensions, like thickness, are in good agreement. However, the agreement gets often worse with higher q values [19, 40–44, 46, 47, 96–98, 109, 110] indicating some differences in detailed electron density profiles [**?**]. For example of the comparison see Fig. 11. The comparison has been usually done based on visual inspection while also quantitative measure for simulated form factor is suggested [22]. In some studies also fourier transform coeffiecients are compared [144**?**]

Also changes in form factor due to temperature [43, 99], cholesterol concentration [97, 98] and acyl chain polyunsaturation [109, 115] has been compared between simulations and experiments [115, 141, 151**?** **?** **?** –153]. Simulation generally reproduce the decreased thickness and increased area with increasing temperature [43, 99] and polyunsaturation level [109, 115], as well as increased thickness and decreased area with increasing cholesterol concentration [97, 98]. However, the temperature dependence is underestimated for some systems [43, 99] while cholesterol effect is overestimated [97, 98]. Example of such comparison is shown in Fig. 11.

In studies where the main goal is to interpret the form factors using MD simulations instead of validating the model, the area per molecule is often fixed to a certain value in order to reproduce the experimental form factor better [143, 147–150]. With this contaraint is indeed, possible to get the form factors close to the experiments, however, careful comparisons between experimental form factors, MD simulations and SDP model suggest small but measurable structural differences [143, 150]. The form factor from the SDP model is in better agreement with simulations and the extracted stuctural parameters indicate differences especially in the headgroup region [143, 150] which is in agreement with the comparions between simulations and NMR order parameter indicating issues in the same region [27], see also section **??**.

In conclusion, all the state of the art simulation models gives form factors close to experimental data in various conditions indicating that the average bilayer dimensions are in good agreement with simulations and experiments. Also the qualitative changes are reproduced, however, sometimes over- or underestimated. In general, the conclusions from scattering data agrees with conclusions from NMR data: the hyd-

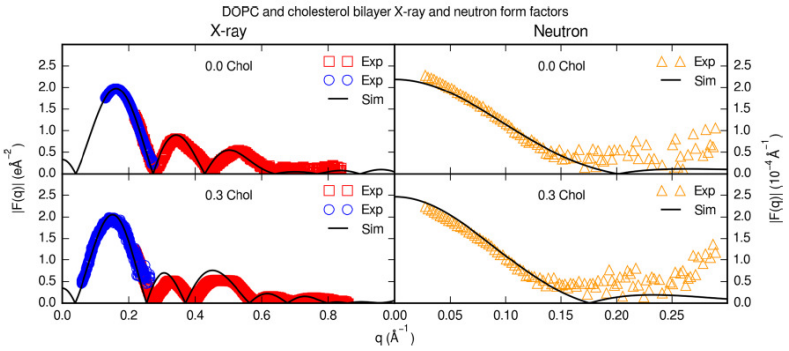

FIG. 11: Example of comparison between simulation model and experiment. The agreement is better with low q values and cholesterol induced thickening is overestimated. Figure adapted from Madej et al. [98].

prohopic acyl chains are often well described in simulations, while in glycerol backbone and headgroup regions there is room for improvement.

9.The more detailed discussion can be found at:

https://github.com/NMRLipids/NMRLipids_V-Review/issues/5

CONCLUSIONS

Recent studies quantitatively comparing atomistic resolution structure and dynamics of lipid bilayer between experiments using C–H bond order parameters, spin relaxation rates and scattering form factors are reviewed. The purpose of these studies is to quantify the atomistic resolution structural and dynamical quality of simulation models as well as to give an atomistic resolution interpretation for the experimental results. For interpretation of these experiments the atomistic resolution MD simulations reproducing all the experiments would be an ultimate tool since the same model can be used to interpret all the experiments. For the same reason, this atomistic resolution model would be most likely a realistic representation for atomistic resolution strucutre and dynamics of lipid bilayers. The main conclusion of this review is that the current MD simulations are not quite yet on the level to perform this task, however, in several aspects indicate that there is potential to improve the models to become truly realistic atomistic resolution representations of these systems.

More specific conclusions are the following:
- The order parameters for each C–H bond in lipid molecules in bilayers can be measured with high quantitative accuracy with both 2H NMR and 13C NMR and this data is available for wide range of lipids in different conditions. Comparison of this data to simulations gives a very detailed picture about the quality of sampled atomistic resolution structures in lipid bilayer and may also help in structural interpretation of experiments. The order parameter changes with varying conditions can be used to study and compare structural changes between simulations and experiments.
- The main conclusions from the comparison of order parameters between experiments and simulations are: 1) the acyl chain structures are generally described realistically for PC lipid bilayers in simulations, 2) the changes in acyl chain region are qualitatively correct but not always quantitatively, 3) the glycerol backbone and choline structures are not within experimental error for any available model and 4) the results depending on structure and energetics of these sections, like ion binding and lipid–cholesterol interactions should be taken with caution.
- The C–H bond rotational dynamics has correct timescale in simulations models for which comparison has been done. Most likely the same applies for all models. However, more careful comparison reveals that, e.g. the glycerol backbone dynamics is too slow in Berger model. Also for CHARMM model all relaxation prosess do not seem to correctly described.
- The development in the scattering methodology has allowed the direct comparison of whole bilayer structure between experimental form factor and simulations. This is complementary to the NMR order parameter which are related to the sampled structures of individual molecules. These comparisons show that the structural lipid bilayer properties like thickness and area per molecule are close to real values, however, it seems that there is room for improvement especially in the lipid headgroup region, in agreement with conclusions from NMR experiments.

When applying lipid bilayer simulations to study complicated biochemical systems it is crusial to recoknize potential artefacts arising from the inaccuracies revealed by these comparisons. Hyphotetical example of a situation where artificial conclusions might be difficult to avoid would be study of protein approaching PC lipid bilayer in physiological NaCl concentration. If the above mentioned issues are not carefully taken into account one might choose a model where the protein is approaching an effectively positively charged lipid bilayer due to artificial Na+ binding with incorrect choline structure. In addition to this the protein might be incorrectly folded already in the bulk water [**?**].

* samuli.ollila@aalto.fi

[1] J. N. Israelachvili, S. Marcelja, and R. G. Horn, Q. Rev. Biophys. **13**, 121 (1980).

[2] R. E. Jacobs and E. Oldfield, Prog. Nucl. Mag. Res. Sp. **14**, 113 (1981).

[3] J. H. Davis, Biochim. Biophys. Acta **737**, 117 (1983).

[4] M. Bloom, E. Evans, and O. G. Mouritsen, Quarterly Reviews of Biophysics **24**, 293 (1991), ISSN 1469-8994, URL http://journals.cambridge.org/article_S0033583500003735.

[5] J. F. Nagle and S. Tristram-Nagle, Biochem. Biophys. Acta **1469**, 159 (2000).

[6] A. G. Lee, Biochim. Biophys. Acta **1666**, 62 (2004).

[7] P. K. J. Kinnunen, The Open Biology Journal **2**, 163 (2009).

[8] P. van der Ploeg and H. J. C. Berendsen, The Journal of Chemical Physics **76** (1982).

[9] R. W. Pastor, R. M. Venable, M. Karplus, and A. Szabo, The Journal of Chemical Physics **89** (1988).

[10] A. Abragam, *The Principles of Nuclear Magnetism* (Oxford University Press, 1961).

[11] A. Seelig and J. Seelig, Biochemistry **13**, 4839 (1974).

[12] H. U. Gally, W. Niederberger, and J. Seelig, Biochemistry **14**, 3647 (1975).

[13] A. Seelig and J. Seelig, Biochemistry **16**, 45 (1977).

[14] J. Seelig and N. Waespe-Sarcevic, Biochemistry **17**, 3310 (1978).

[15] L. Strenk, P. Westerman, and J. Doane, Biophys. J. **48**, 765 (1985).

[16] J. E. Baenziger, H. C. Jarrel, R. J. Hill, and I. C. P. Smith, Biochemistry **30**, 894 (1991).

[17] M. Hong, K. Schmidt-Rohr, and D. Nanz, Biophys. J. **69**, 1939 (1995).

[18] K. S. Bruzik and J. S. Harwood, Journal of the American Chemical Society **119**, 6629 (1997).

[19] J. Chowdhary, E. Harder, P. E. M. Lopes, L. Huang, A. D. MacKerell, and B. Roux, J. Phys. Chem. B **117**, 9142 (2013).

[20] P. Prakash and R. Sankararamakrishnan, J. Comp. Chem. **31**, 266 (2010).

[21] T. M. Ferreira, O. H. S. Ollila, R. Pigliapochi, A. P. Dabkowska, and D. Topgaard, J. Chem. Phys. **142**, 044905 (2015), URL http://scitation.aip.org/content/aip/journal/jcp/142/4/10.1063/1.4906274.

[22] N. Kuerka, J. Katsaras, and J. Nagle, Journal of Membrane Biology **235**, 43 (2010), ISSN 0022-2631.

[23] J. Seelig, Q. Rev. Biophys. **10**, 353 (1977).

[24] J. D. Gross, D. E. Warschawski, and R. G. Griffin, J. Am. Chem. Soc. **119**, 796 (1997).

[25] S. V. Dvinskikh, V. Castro, and D. Sandstrom, Phys. Chem. Chem. Phys. **7**, 607 (2005).

[26] T. M. Ferreira, F. Coreta-Gomes, O. H. S. Ollila, M. J. Moreno, W. L. C. Vaz, and D. Topgaard, Phys. Chem. Chem. Phys. **15**, 1976 (2013).

[27] A. Botan, F. Fernando, J. F. Patrick Franois, M. Javanainen, M. Kanduc, W. Kulig, A. Lamberg, C. Loison, A. P. Lyubartsev, M. S. Miettinen, et al., The Journal of Physical Chemistry B **0**, null (0), pMID: 26509669, http://dx.doi.org/10.1021/acs.jpcb.5b04878, URL http://dx.doi.org/10.1021/acs.jpcb.5b04878.

[28] M. Hong, K. Schmidt-Rohr, and A. Pines, J. Am. Chem. Soc. **117**, 3310 (1995).

[29] A. Seelig and J. Seelig, Biochimica et Biophysica Acta (BBA) - Biomembranes **406**, 1 (1975).

[30] H. U. Gally, G. Pluschke, P. Overath, and J. Seelig, Biochemistry **20**, 1826 (1981).

[31] A. K. Engel and D. Cowburn, FEBS Letters **126**, 169 (1981).

[32] B. Perly, I. C. P. Smith, and H. C. Jarrell, Biochemistry **24**, 1055 (1985).

[33] H. Akutsu and J. Seelig, Biochemistry **20**, 7366 (1981).

[34] B. Bechinger and J. Seelig, Chem. Phys. Lipids **58**, 1 (1991).

[35] O. Berger, O. Edholm, and F. Jähnig, Biophys. J. **72**, 2002 (1997).

[36] C.-J. Högberg, A. M. Nikitin, and A. P. Lyubartsev, J. Comput. Chem. **29**, 2359 (2008).

[37] D. Poger, W. F. Van Gunsteren, and A. E. Mark, J. Comput. Chem. **31**, 1117 (2010).

[38] J. P. Ulmschneider and M. B. Ulmschneider, J. Chem. Theory Comput. **5**, 1803 (2009).

[39] A. Kukol, J. Chem. Theory Comput. **5**, 615 (2009).

[40] S.-W. Chiu, S. A. Pandit, H. L. Scott, and E. Jakobsson, J. Phys. Chem. B **113**, 2748 (2009).

[41] J. B. Klauda, R. M. Venable, J. A. Freites, J. W. O'Connor, D. J. Tobias, C. Mondragon-Ramirez, I. Vorobyov, A. D. M. Jr, and R. W. Pastor, J. Phys. Chem. B **114**, 7830 (2010).

[42] C. J. Dickson, L. Rosso, R. M. Betz, R. C. Walker, and I. R. Gould, Soft Matter **8**, 9617 (2012).

[43] J. P. M. Jämbeck and A. P. Lyubartsev, J. Phys. Chem. B **116**, 3164 (2012).

[44] A. Maciejewski, M. Pasenkiewicz-Gierula, O. Cramariuc, I. Vattulainen, and T. Rog, J. Phys. Chem. B **118**, 4571 (2014).

[45] R. Tjörnhammar and O. Edholm, J. Chem. Theory Comput. **10**, 5706 (2014).

[46] C. J. Dickson, B. D. Madej, . A. Skjevik, R. M. Betz, K. Teigen, I. R. Gould, and R. C. Walker, J. Chem. Theory Comput. **10**, 865 (2014).

[47] S. Lee, A. Tran, M. Allsopp, J. B. Lim, J. Henin, and J. B. Klauda, J. Phys. Chem. B **118**, 547 (2014).

[48] V. Castro, S. V. Dvinskikh, G. Widmalm, D. Sandstrm, and A. Maliniak, Biochimica et Biophysica Acta (BBA) - Biomembranes **1768**, 2432 (2007).

[49] V. Castro, B. Stevensson, S. V. Dvinskikh, C.-J. Högberg, A. P. Lyubartsev, H. Zimmermann, D. Sandström, and A. Maliniak, Biochim. Biophys. Acta - Biomembranes **1778**, 2604 (2008).

[50] A. Leftin and M. F. Brown, Biochim. Biophys. Acta - Biomembranes **1808**, 818 (2011).

[51] D. Marsh, *Handbook of Lipid Bilayers, Second Edition* (RSC press, 2013).

[52] Journal of Molecular Biology **425**, 2973 (2013).

[53] A. Leftin, T. Molugu, C. Job, K. Beyer, and M. Brown, Biophysical Journal **107**, 2274 (2014).

[54] A. Ulrich and A. Watts, Biophys. J. **66**, 1441 (1994).

[55] K. Mallikarjunaiah, A. Leftin, J. J. Kinnun, M. J. Justice, A. L. Rogozea, H. I. Petrache, and M. F. Brown, Biophysical Journal **100**, 98 (2011), ISSN 0006-3495, URL http://www.sciencedirect.com/science/article/pii/S0006349510013792.

[56] C. Altenbach and J. Seelig, Biochemistry **23**, 3913 (1984).

[57] J. Seelig, P. M. MacDonald, and P. G. Scherer, Biochemistry **26**, 7535 (1987).

[58] P. G. Scherer and J. Seelig, Biochemistry **28**, 7720 (1989).

[59] M. F. Brown and J. Seelig, Biochemistry **17**, 381 (1978).

[60] J. Douliez, A. Lonard, and E. Dufourc, Biophysical Journal **68**, 1727 (1995), ISSN 0006-3495, URL http://www.sciencedirect.com/science/article/pii/S0006349595803504.

[61] E. Kuchinka and J. Seelig, Biochemistry **28**, 4216 (1989).

[62] M. Roux and M. Bloom, Biochemistry **29**, 7077 (1990).

[63] A. Catte, M. Girych, M. Javanainen, M. S. Miettinen, L. Monticelli, J. Määttä, V. S. Oganesyan, and O. H. S. Ollila, *The electrometer concept and binding of cations to phospholipid bilayers* (2015), dOI: 10.5281/zenodo.32175.

[64] F. Aussenac, M. Laguerre, J.-M. Schmitter, and E. J. Dufourc, Langmuir **19**, 10468 (2003).

[65] G. Raffard, S. Steinbruckner, A. Arnold, J. H. Davis, and E. J. Dufourc, Langmuir **16**, 7655 (2000).

[66] C. R. Sanders and J. P. Schwonek, Biochemistry **31**, 8898 (1992).

[67] L. E. Marbella, B. Yin, and M. M. Spence, The Journal of Physical Chemistry B **119**, 4194 (2015).

[68] J. Becker, A. Comotti, R. Simonutti, P. Sozzani, and K. Saalwchter, The Journal of Physical Chemistry B **109**, 23285 (2005).

[69] V. N. Sivanandam, J. Cai, A. G. Redfield, and M. F. Roberts, Journal of the American Chemical Society **131**, 3420 (2009).

[70] S. V. Dvinskikh, V. Castro, and D. Sandstrom, Phys. Chem. Chem. Phys. **7**, 3255 (2005).

[71] C.-J. Hgberg, , and A. P. Lyubartsev*, The Journal of Physical Chemistry B **110**, 14326 (2006).

[72] *The nmrlipids project, on the signs of the order parameters* (2014), URL http://web.archive.org/web/20150414085027/http://nmrlipids.blogspot.fi/2014/04/on-signs-of-order-parameters.html.

[73] S. Ollila, M. T. Hyvönen, and I. Vattulainen, J. Phys. Chem. B **111**, 3139 (2007).

[74] D. P. Tieleman, S. J. Marrink, and H. J. C. Berendsen, Biochim. Biophys. Acta **1331**, 235 (1997).

[75] L. Vermeer, B. de Groot, V. Rat, A. Milon, and J. Czaplicki, Eur. Biophys. J. **36**, 919 (2007), ISSN 0175-7571, URL http://dx.doi.org/10.1007/s00249-007-0192-9.

[76] D. Poger and A. E. Mark, J. Chem. Theory Comput. **8**, 4807 (2012).

[77] M. Bachar, P. Brunelle, D. P. Tieleman, and A. Rauk, J. Phys. Chem. B **108**, 7170 (2004).

[78] J. Wong-ekkabut, Z. Xu, W. Triampo, I.-M. Tang, D. P. Tieleman, and L. Monticelli, Biophysical Journal **93**, 4225 (2007), ISSN 0006-3495, URL http://www.sciencedirect.com/science/article/pii/S0006349507716752.

[79] A. Vogel and S. Feller, The Journal of Membrane Biology **245**, 23 (2012), ISSN 0022-2631.

[80] E. Egberts and H. J. C. Berendsen, J. Chem. Phys. **89**, 3718 (1988).

[81] T. R. Stouch, Molecular Simulation **10**, 335 (1993).

[82] E. Egberts, S.-J. Marrink, and H. Berendsen, European Biophysics Journal **22**, 423 (1994), ISSN 0175-7571, URL http://dx.doi.org/10.1007/BF00180163.

[83] J. W. Essex, M. M. Hann, and W. G. Richards, Philos. T. Roy. Soc. B **344**, 239 (1994).

[84] A. Robinson, W. Richards, P. Thomas, and M. Hann, Biophys. J. **67**, 2345 (1994).

[85] M. T. Hyvönen, M. Ala-Korpela, J. Vaara, T. T. Rantala, and J. Jokisaari, Chem. Phys. Lett. **246**, 300 (1995).

[86] V. Kothekar, Ind. J. Biochem. Biophys. **33**, 431 (1996).

[87] D. P. Tieleman and H. J. C. Berendsen, J. Chem. Phys. **105**, 4871 (1996).

[88] W. Shinoda, N. Namiki, and S. Okazaki, J. Chem. Phys. **106**, 5731 (1997).

[89] J. B. Klauda, R. M. Venable, A. D. M. Jr., and R. W. Pastor, in *Computational Modeling of Membrane Bilayers*, edited by S. E. Feller (Academic Press, 2008), vol. 60 of *Current Topics in Membranes*, pp. 1 – 48.

[90] S. W. I. Siu, R. Vcha, P. Jungwirth, and R. A. Bckmann, The Journal of Chemical Physics **128** (2008).

[91] E. J. Dufourc, E. J. Parish, S. Chitrakorn, and I. C. P. Smith, Biochemistry **23**, 6062 (1984).

[92] M. Lafleur, P. Cullis, and M. Bloom, European Biophysics Journal **19**, 55 (1990), ISSN 0175-7571, URL http://dx.doi.org/10.1007/BF00185086.

[93] J. A. Urbina, S. Pekerar, H. biao Le, J. Patterson, B. Montez, and E. Oldfield, Biochimica et Biophysica Acta (BBA) - Biomembranes **1238**, 163 (1995), ISSN 0005-2736, URL http://www.sciencedirect.com/science/article/pii/000527369500117L.

[94] R. J. Mashl, H. L. Scott, S. Subramaniam, and E. Jakobsson, Biophys. J. **81**, 3005 (2001).

[95] Q. Zhu, K. H. Cheng, and M. W. Vaughn, J. Phys. Chem. B **111**, 11021 (2007).

[96] J. B. Lim, B. Rogaski, and J. B. Klauda, J. Phys. Chem. B **116**, 203 (2012).

[97] J. P. M. Jambeck and A. P. Lyubartsev, Phys. Chem. Chem. Phys. **15**, 4677 (2013).

[98] B. D. Madej, I. R. Gould, and R. C. Walker, The Journal of Physical Chemistry B **119**, 12424 (2015).

[99] X. Zhuang, J. R. Makover, W. Im, and J. B. Klauda, Biochimica et Biophysica Acta (BBA) - Biomembranes **1838**, 2520 (2014).

[100] M. Höltje, T. Förster, B. Brandt, T. Engels, W. von Rybinski, and H.-D. Höltje, Biochim. Biophys. Acta **1511**, 156 (2001).

[101] M. T. Hyvönen, T. T. Rantala, and M. Ala-Korpela, Biophys. J. **73**, 2907 (1997).

[102] M. Hyvnen, M. Ala-Korpela, J. Vaara, T. T. Rantala, and J. Jokisaari, Chemical Physics Letters **268**, 55 (1997), ISSN 0009-2614, URL http://www.sciencedirect.com/science/article/pii/S0009261497001711.

[103] S. Feller, D. Yin, R. Pastor, and A. M. Jr, Biophysical Journal **73**, 2269 (1997).

[104] L. Saiz and M. L. Klein, Biophys. J. **204**, 204 (2001).

[105] T. Huber, K. Rajamoorthi, V. F. Kurze, K. Beyer, and M. F. Brown, J. Am. Chem. Soc. **124**, 298 (2002).

[106] S. E. Feller, K. Gawrisch, and A. D. MacKerell Jr., J. Am. Chem. Soc. **124**, 318 (2002).

[107] T. Rg, K. Murzyn, R. Gurbiel, Y. Takaoka, A. Kusumi, and M. Pasenkiewicz-Gierula, Journal of Lipid Research **45**, 326 (2004).

[108] M. T. Hyvönen and P. T. Kovanen, Eur. Biophys. J. **34**, 294 (2005).

[109] J. B. Klauda, V. Monje, T. Kim, and W. Im, The Journal of Physical Chemistry B **116**, 9424 (2012).

[110] W. Kulig, M. Pasenkiewicz-Gierula, and T. Róg, Chem. Phys. Lipids pp. *In Press, Accepted Manuscript, http://dx.doi.org/10.1016/j.chemphyslip.2015.07.002* (2015), URL http://www.sciencedirect.com/science/article/pii/S0009308415300074.

[111] H. I. Petrache, S. W. Dodd, and M. F. Brown, Biophys. J. **79**, 3172 (2000).

[112] K. Rajamoorthi and M. F. Brown, Biochemistry **30**, 4204 (1991).

[113] J. Kapla, B. Stevensson, M. Dahlberg, and A. Maliniak, J. Phys. Chem. B **116**, 244 (2012).

[114] H. Schindler and J. Seelig, Biochemistry **14**, 2283 (1975).

[115] N. V. Eldho, S. E. Feller, S. Tristram-Nagle, I. V. Polozov, and

K. Gawrisch, J. Am. Chem. Soc. **125**, 6409 (2003).
[116] W. Stillwell and S. R. Wassall, Chem. Phys. Lipids **126**, 1 (2003).
[117] K. Gawrisch, N. V. Eldho, and L. L. Holte, Lipids **38**, 445 (2003).
[118] J. H. Ipsen, G. Karlstrm, O. Mourtisen, H. Wennerstrm, and M. Zuckermann, Biochimica et Biophysica Acta (BBA) - Biomembranes **905**, 162 (1987).
[119] K. Gawrisch, D. Ruston, J. Zimmerberg, V. Parsegian, R. Rand, and N. Fuller, Biophysical Journal **61**, 1213 (1992).
[120] H. Akutsu and T. Nagamori, Biochemistry **30**, 4510 (1991).
[121] D. J. Semchyschyn and P. M. Macdonald, Magn. Res. Chem. **42**, 89 (2004).
[122] A. Arkhipov, Y. Shan, R. Das, N. Endres, M. Eastwood, D. Wemmer, J. Kuriyan, and D. Shaw, Cell **152**, 557 (2013).
[123] K. Kaszuba, M. Grzybek, A. Orowski, R. Danne, T. Rg, K. Simons, . Coskun, and I. Vattulainen, Proceedings of the National Academy of Sciences **112**, 4334 (2015).
[124] G. Lipari and A. Szabo, J. Am. Chem. Soc. **104**, 4546 (1982).
[125] A. Nowacka, P. C. Mohr, J. Norrman, R. W. Martin, and D. Topgaard, Langmuir **26**, 16848 (2010).
[126] J. Hirschinger, Concept. Magn. Reson. A **28A**, 307 (2006).
[127] E. Lindahl and O. Edholm, J. Chem. Phys. **115**, 4938 (2001).
[128] J. Wohlert, W. K. den Otter, O. Edholm, and W. J. Briels, J. Chem. Phys. **124**, 154905 (2006).
[129] M. Abraham, D. van der Spoel, E. Lindahl, B. Hess, and the GROMACS development team, *GROMACS user manual version 5.0.7* (2015), URL `www.gromacs.org`.
[130] R. W. Pastor*, , R. M. Venable, and S. E. Feller, Accounts of Chemical Research **35**, 438 (2002).
[131] R. Venable, Y. Zhang, B. Hardy, and R. Pastor, Science **262**, 223 (1993).
[132] O. Edholm, in *Computational Modeling of Membrane Bilayers*, edited by S. E. Feller (Academic Press, 2008), vol. 60 of *Current Topics in Membranes*, pp. 91 – 110.
[133] J. B. Klauda, N. V. Eldho, , K. Gawrisch, B. R. Brooks, , and R. W. Pastor*, The Journal of Physical Chemistry B **112**, 5924 (2008).
[134] J. B. Klauda, M. F. Roberts, A. G. Redfield, B. R. Brooks, and R. W. Pastor, Biophysical Journal **94**, 3074 (2008), ISSN 0006-3495, URL `http://www.sciencedirect.com/science/article/pii/S0006349508704648`.
[135] S. E. Feller, D. Huster, , and K. Gawrisch, Journal of the American Chemical Society **121**, 8963 (1999).
[136] M. F. Roberts, , and . Alfred G. Redfield*, Journal of the American Chemical Society **126**, 13765 (2004).
[137] M. F. Roberts and A. G. Redfield, Proceedings of the National Academy of Sciences of the United States of America **101**, 17066 (2004).
[138] M. F. Roberts, A. G. Redfield, and U. Mohanty, Biophys. J. **97**, 132 (2009).
[139] A. Nowacka, N. Bongartz, O. Ollila, T. Nylander, and D. Topgaard, Journal of Magnetic Resonance **230**, 165 (2013).
[140] T. M. Ferreira, Ph.D. thesis, Lund University, http://lup.lub.lu.se/record/3878850/file/3879121.pdf (2013).
[141] N. Kuerka, Y. Liu, N. Chu, H. I. Petrache, S. Tristram-Nagle, and J. F. Nagle, Biophysical Journal **88**, 2626 (2005).
[142] N. Kuerka, J. Pencer, J. N. Sachs, J. F. Nagle, and J. Katsaras, Langmuir **23**, 1292 (2007).
[143] N. Kuerka, J. F. Nagle, J. N. Sachs, S. E. Feller, J. Pencer, A. Jackson, and J. Katsaras, Biophysical Journal **95**, 2356 (2008).
[144] R. W. Benz, F. Castro-Romn, D. J. Tobias, and S. H. White, Biophysical Journal **88**, 805 (2005).
[145] A. Braun, E. Brandt, O. Edholm, J. Nagle, and J. Sachs, Biophysical Journal **100**, 2112 (2011).
[146] (????).
[147] J. N. Sachs, H. I. Petrache, and T. B. Woolf, Chemistry and Physics of Lipids **126**, 211 (2003).
[148] J. B. Klauda, N. Kuerka, B. R. Brooks, R. W. Pastor, and J. F. Nagle, Biophysical Journal **90**, 2796 (2006).
[149] N. Kuerka, J. D. Perlmutter, J. Pan, S. Tristram-Nagle, J. Katsaras, and J. N. Sachs, Biophysical Journal **95**, 2792 (2008).
[150] A. R. Braun, J. N. Sachs, and J. F. Nagle, The Journal of Physical Chemistry B **117**, 5065 (2013).
[151] J. Pan, T. T. Mills, S. Tristram-Nagle, and J. F. Nagle, Phys. Rev. Lett. **100**, 198103 (2008).
[152] N. Kucerka, J. F. Nagle, J. N. Sachs, S. E. Feller, J. Pencer, A. Jackson, and J. Katsaras, Biophys. J. **95**, 2356 (2008), ISSN 0006-3495, URL `http://www.sciencedirect.com/science/article/B94RW-4VB4SVM-S/2/7ede236c4e83d16a6fe57cc3b1894349`.
[153] J. Pan, S. Tristram-Nagle, and J. F. Nagle, Phys. Rev. E **80**, 021931 (2009).

ToDo